land

MDPI

Article

Soil Texture Mapping in the Permafrost Region: A Case Study on the Eastern Qinghai–Tibet Plateau

Wangping Li [1,2,3], Yadong Liu [3,4,5,*], Xiaodong Wu [3,4,5], Lin Zhao [3,6], Tonghua Wu [3,4], Guojie Hu [3,4], Defu Zou [3,4], Yongping Qiao [3,4], Xiaoying Fan [3,4,5] and Xiaoxian Wang [1,2]

1 School of Civil Engineering, Lanzhou University of Technology, Lanzhou 730050, China; wxiaoxian2024@lzu.edu.cn (X.W.)
2 Emergency Mapping Engineering Research Center of Gansu, Lanzhou 730050, China
3 Cryosphere Research Station on the Qinghai-Tibet Plateau, State Key Laboratory of Cryospheric Science, Northwest Institute of Eco-Environment and Resource, Chinese Academy of Sciences, Lanzhou 730000, China; wuxd@lzb.ac.cn (X.W.); lzhao@nuist.edu.cn (L.Z.); thuawu@lzb.ac.cn (T.W.); huguojie123@lzb.ac.cn (G.H.); defuzou@lzb.ac.cn (D.Z.); qyp@lzb.ac.cn (Y.Q.); fanxiaoyin@nieer.ac.cn (X.F.)
4 Cryosphere Research Station on the Qinghai-Tibet Plateau, Key Laboratory of Cryospheric Science and Frozen Soil Engineering, Northwest Institute of Eco-Environment and Resources, Chinese Academy of Sciences, Lanzhou 730000, China
5 University of Chinese Academy Sciences, Beijing 100049, China
6 School of Geographical Sciences, Nanjing University of Information Science & Technology, Nanjing 210044, China
* Correspondence: liuyadong@nieer.ac.cn

Abstract: Soil particle distribution is one of the basic parameters for many Earth system models, while the soil texture data are largely not available. This is especially true for complex terrains due to the difficulties in data acquisition. Here, we selected an area, Wenquan area, with rolling mountains and valleys, in the eastern Qinghai–Tibet Plateau (QTP) as the study area. Using the random forest model, we established quantitative models of silt, clay, and sand content, and environmental variables, including elevation, slope, aspect, plane curvature, slope curvature, topographic wetness index, NDVI, EVI, MAT, and MAP at different depths based on the survey data of 58 soil sample points. The results showed that sand content was the highest, accounting for more than 75% of the soil particles. Overall, the average values of clay and silt gradually decreased with increasing soil profile depth, while sand showed the opposite pattern. In terms of spatial distribution, clay and silt are higher in the southeast and lower in the northwest in each standard layer, while sand is just the opposite. The random forest regression model showed that vegetation condition was a controlling factor of soil particle size. These results showed that random forest applies to predicting the spatial distribution of soil particle sizes for areas with complex terrains.

Keywords: permafrost; machine learning; digital soil mapping; soil particle size distribution

check for updates

Citation: Li, W.; Liu, Y.; Wu, X.; Zhao, L.; Wu, T.; Hu, G.; Zou, D.; Qiao, Y.; Fan, X.; Wang, X. Soil Texture Mapping in the Permafrost Region: A Case Study on the Eastern Qinghai–Tibet Plateau. *Land* **2024**, *13*, 1855. https://doi.org/10.3390/land13111855

Academic Editor: Richard Smardon

Received: 25 September 2024
Revised: 31 October 2024
Accepted: 6 November 2024
Published: 7 November 2024

Copyright: © 2024 by the authors. Licensee MDPI, Basel, Switzerland. This article is an open access article distributed under the terms and conditions of the Creative Commons Attribution (CC BY) license (https://creativecommons.org/licenses/by/4.0/).

1. Introduction

Soil texture describes the ratio of clay, silt, and sand particles present within the soil [1,2]. It is a fundamental physical characteristic of soil [3,4]. It is strongly linked to various soil properties, including saturated water content, hydraulic conductivity, soil organic carbon, and thermal conductivity [5–7]. In addition, soil texture serves as a fundamental input for various Earth system models and plays a crucial role in the accurate simulation of land surface process models and biogeochemical cycle models [8–10]. These models rely on soil texture data to predict the transfer of water, energy, and nutrients, thereby enhancing our understanding and simulation of ecosystem dynamics.

Permafrost is a significant element of the Earth's cryospheric system [11]. Areas characterized by permafrost cover a substantial portion of the land in the Northern Hemisphere [12]. Since the 1980s, permafrost regions have been warming twice as fast at the global average [13].

Formed in cold climates, permafrost is highly responsive to rising temperatures [14]. On a global scale, permafrost degradation has been widely recorded [15–17]. The melting of permafrost can generate feedback effects on climate warming through alterations in ecosystems, water systems, and the carbon cycle [18]. Therefore, modeling permafrost change is an important step toward developing climate change adaptation strategies. Presently, the lack of spatial distribution data on soil texture is one of the barriers to modeling the permafrost change [19]. Due to the soil texture controlling soil moisture, soil organic carbon stabilization, and soil heat conductivity, which are important parameters for permafrost modeling [20–22], there is an urgent need to create soil texture data at the regional scale. However, in permafrost regions, the soil texture distribution is mainly based on the data from soil sample points at the site scale [23]. It has been well recognized that many permafrost regions are characterized by complex terrains [24,25], and therefore, determining the spatial distribution of soil texture in permafrost areas continues to be a major challenge.

The early soil texture spatial prediction mapping primarily relied on traditional statistical methods. These methods used the statistical relationships of sampling point data for spatial interpolation to generate soil texture distribution maps. For example, based on the texture profile data and using the polygon linking method, a soil texture map with a 1 km resolution has been created in China [26]. Using regression kriging and multiple linear regression, the soil particle distribution in Gadag district in Karnataka, India, was predicted [27]. Based on limited soil sample data, a comparison was made between multiple stepwise regression (MSR) methods in the application of soil texture spatial mapping [28]. However, traditional statistical methods often have limited ability to capture the spatial heterogeneity and nonlinear relationships in the data, making it difficult to accurately represent the complex variations in soil texture [29,30].

In recent years, digital soil mapping techniques, driven by modern data-driven methods such as machine learning, have rapidly advanced in applications for spatial prediction of soil texture. Digital soil mapping refers to methods that use geographic information systems, remote sensing data, statistical models, and machine learning techniques to predict and map soil attributes spatially [31]. Techniques like random forests, support vector machines, and neural networks have improved prediction accuracy and efficiency through training on large volumes of data. For example, using the random forest model, the spatial variations of sand, silt, and clay contents across China at the 90 m resolution have been predicted [32]. During 2009–2013, the Global SoilMap project was performed to provide a global grid of soil functional properties, including soil textures, using machine learning methods [33]. By adjusting the parameters of convolutional neural networks (CNNs), the accuracy of soil texture predictions can be significantly improved [34]. Overall, these advancements highlight the growing importance of incorporating sophisticated computational techniques into soil science research to achieve more precise and reliable predictions.

In this study, we selected a permafrost region in the eastern QTP, a typical permafrost within complex terrains, as a study area. The main goals of this study are to (1) investigate the soil texture distribution data using the random forest model and (2) investigate how soil texture relates to environmental factors. The findings will provide a scientific basis for mapping soil texture in permafrost regions with complex terrains, and thus would be helpful to develop and improve the Earth system models.

2. Material and Methods

2.1. Study Area

The Wenquan area (35°06′~35°42′ N, 99°06′~99°42′ E), located at the eastern boundary of the permafrost region on the QTP, exemplifies the cold-temperate continental climate and is representative of permafrost, cold-region soils, and cold-region ecosystems (Figure 1). This area consists of rolling mountains with valleys and basins. The elevation ranges from 3424 to 5305 m, with a mean elevation of about 4300 m. From 1961 to 2000, the mean annual temperature was about −3.2 °C, and the average annual precipitation was 500~600 mm [35]. According to the field survey in 2009 and follow-up surveys in recent years, it was found

that the study area is mainly dominated by grassland ecosystems. The main vegetation type is alpine grassland.

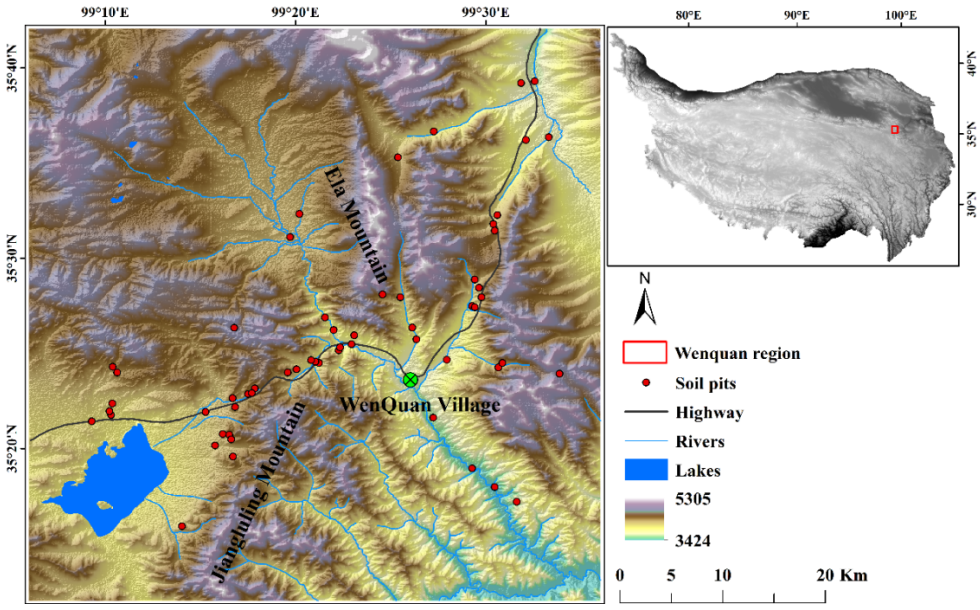

Figure 1. The study region along with the locations of the sampling sites.

2.2. Field Work

We conducted extensive field surveys in the area, primarily including soil and vegetation investigations (Figure 2). Based on vegetation type, soil type, and road accessibility in the study area, we obtained 73 soil profiles, but only 58 soil profiles were deeper than 1 m. In the actual survey, detailed information was recorded for each soil sample point, including longitude, latitude, soil type, pH, Mg^{2+}, Na^{+}, TP, TN, etc. Soil property information for some typical survey sites is presented in Table 1. The soil particles were measured by a combination of wet sieving [36] and a particle size analyzer (Sedimat 4–12, UGT, Berlin, Germany). Particles smaller than 2 µm were classified as clay, those ranging from 2 to 50 µm were categorized as silt, and particles between 50 and 2000 µm were identified as sand [37].

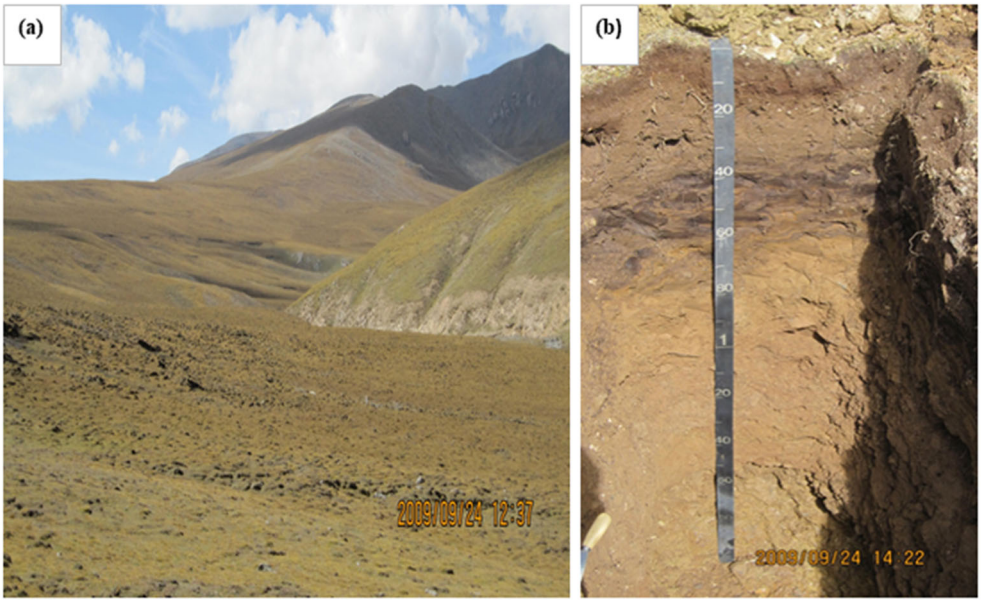

Figure 2. Photographs from the field illustrating (**a**) the collection of soil samples and (**b**) a profile of the soil.

Table 1. Basic physical information of five typical sampling points.

Soils	Coordinates (N)	Coordinates (E)	Elevation (m)	Slope (°)	Aspect (°)	Layers	Depth (cm)	PH (%)	TN (%)	TP (%)	TK (%)	Mg^{2+} (mg/kg)	Na^{+} (mg/kg)
IEFK (Pachic Haplocryolls)	35.46	99.49	4200	4	260	A1	0–15	7.66	0.380	0.040	1.700	29.26	3.73
						A2	15–40	7.97	0.375	0.040	1.440	42.59	176.00
						A3	40–50	8.03	0.274	0.037	1.420	125.19	65.44
						2Bk	50–100	8.23	0.085	0.012	1.760	34.32	73.19
						2Cr	100–215	8.30	0.063	0.007	1.910	75.05	40.52
IEFP (Typic Haplocryolls)	35.46	99.49	4240	2	300	A	0–30	8.02	0.168	0.045	1.060	79.06	92.81
						2Bw1	30–80	9.02	0.076	0.006	0.990	158.29	311.67
						2Bw2	80–110	8.72	0.092	0.009	0.800	91.23	319.60
						2Cr	110–200	9.52	0.063	0.006	0.940	54.74	265.69
KDAO (Typic Humicryepts)	35.48	99.49	4334	13	225	A	0–25	8.02	0.183	0.055	1.300	67.05	34.99
						Bw	25–90	7.97	0.095	0.033	1.310	36.48	33.66
						Crk/B	90–120	8.04	0.09	0.055	1.600	36.53	35.29
						Crk	120–330	8.08	0.059	0.062	1.540	54.82	47.46
KDAN (Eutric Humicryepts)	35.54	99.51	4247	6	110	A1	0–5	6.72	0.800	0.067	1.600	49.54	6.18
						A2	5–16	7.10	0.704	0.084	1.500	23.17	6.26
						Bg1	16–30	7.10	0.257	0.050	1.320	46.54	1.26
						2Bg2	30–50	7.27	0.196	0.057	1.700	6.08	1.27
						2Bw	50–100	7.82	0.048	0.060	1.620	8.51	6.20
						2C	100–220	7.90	0.048	0.070	1.380	26.75	1.26
KDDM9 (Fluventic Haplocryepts)	35.66	99.54	3884	0.5	10	A	0–5	7.61	0.327	0.051	0.970	55.26	21.01
						Bw	5–10	7.60	0.154	0.055	1.530	41.43	61.02
						Ab1	10–23	7.63	0.673	0.061	1.100	80.42	100.64
						Bwb1	23–52	7.84	0.138	0.048	1.480	43.90	21.00
						Ab2	52–65	7.85	0.290	0.051	1.560	51.11	18.52
						Bwb2	65–95	7.44	0.073	0.045	1.770	14.60	1.27
						Bgb2	95–200	7.27	0.108	0.042	2.090	20.67	8.65

2.3. Environmental Covariates

Soil is a product of the comprehensive interaction of climate, biology, topography, and parent material over time [38]. Since the parent materials are non-quantified data, we included three types of environmental variables: climate, biology, and topography. We chose covariates related to the processes of soil particle formation, accumulation, and transport, as well as those that indicate spatial variations in soil texture (Table 2).

Table 2. Environmental factors used to describe the formative elements of soil texture prediction (c: climate, r: relief, o: organisms).

Predictor	Description	Resolution	Factors
Elevation	Elevation above sea level (m)	30 m	r
Aspect	Aspect gradient	30 m	r
Slope	Slope gradient	30 m	r
Plan	Plan curvature	30 m	r
Profile	Profile curvature	30 m	r
TWI	topographic wetness index	30 m	r
MAP	Annual precipitation (mm)	1 km	c
MAT	Annual mean temperature (°C)	1 km	c
NDVI	Mean NDVI during the growing season	30 m	o, c
EVI	Enhanced Vegetation Index	30 m	o, c

The latitude and longitude data of the soil pedons were recorded using a handheld GPS instrument. The MODIS data were downloaded from the NASA remote sensing data website (https://ladsweb.modaps.eosdis.nasa.gov). The data format conversion, splicing, projection conversion, and resampling were processed to obtain the Normalized Differential Vegetation Index (NDVI) and Enhanced Vegetation Index (EVI) data. According to the 30 m SRTM-DEM provided by CGIAR-CSI, the elevation, slope, aspect, topographic wetness index, plan curvature, and profile curvature for each sampling site were obtained. The mean annual air temperature (MAT) and mean annual precipitation (MAP) data were downloaded from WorldClim version 2.1 (https://www.worldclim.org).

2.4. Random Forest Model

The random forest model was developed on the basis of a decision tree [39,40]. The random forest was proposed in 2001. It is a nonlinear modeling tool with high prediction accuracy and avoids overfitting [41]. The model can also obtain the importance of variables [42,43]. Random forest modeling and mapping can be conducted within the R environment using the 'randomForest' package [44,45]. In the R environment, the random forest regression model employs the %IncMSE metric to indicate the significance of variables [46]. A higher %IncMSE value indicates that the environmental variables hold greater significance in the model [47].

2.5. Data Processing and Analysis

There are 58 standardized pedons with depths larger than 1 m. The soil samples were collected at different depth intervals, i.e., 0–5 cm, 5–15 cm, 15–30 cm, 30–60 cm, 60–100 cm, and 100–200 cm. The soil particle distribution of these layers was analyzed.

For the pixel scale, the sum of clay, silt, and sand is 100%. Therefore, for the spatial distribution map of clay, silt, and sand obtained by the random forest model, we performed post-processing to ensure that the sum of soil textures on a single pixel is 100%, as shown in Equation (1).

$$\mathrm{Sand}_c[\%] = \frac{\mathrm{Sand}}{(\mathrm{Sand} + \mathrm{Silt} + \mathrm{Clay})} \cdot 100 \quad (1)$$

2.6. Accuracy Validation

$$R^2 = 1 - \frac{\sum_{i=1}^{n}(\rho_i - o_i)^2}{\sum_{i=1}^{n}(\rho_i - \hat{o})^2} \quad (2)$$

$$ME = \frac{1}{n}\sum_{i=1}^{n}(o_i - \rho_i) \quad (3)$$

$$RMSE = \sqrt{\frac{1}{n}\sum_{i=1}^{n}(\rho_i - \sigma_i)^2} \quad (4)$$

The ρ_i and o_i are the predicted and observed values of soil texture fractions at sample site i; $\hat{o}$ is the average observation value.

3. Results

3.1. Soil Particle Distribution

The fraction of sand in the Wenquan area accounted for more than 75% of the total particles (Table 3). The mean sand slightly increased with depth, while the mean clay and silt contents slightly decreased with depth. The clay and silt contents had great variabilities for all depth layers, with the coefficient of variation (CV) between 0.34 and 0.66, whereas sand content had lower variability, with the CVs ranging from 0.08 to 0.13. From the kurtosis and skewness values of soil clay, silt, and sand at each level, it was found that they basically obey the normal distribution.

Table 3. Analysis of the statistical characteristics of soil profile data.

Depth (cm)	Min (%)	Max (%)	Mean (%)	SD (%)	CV	Skewness	Kurtosis
Clay							
0–5	3.77	26.35	15.27	5.39	0.35	0.09	−0.84
5–15	3.77	32.66	15.19	6.08	0.40	0.51	−0.17
15–30	2.99	27.93	12.13	5.93	0.49	0.73	−0.03
30–60	1.02	19.65	9.54	4.76	0.50	0.58	−0.74
60–100	1.75	17.54	7.51	3.98	0.53	0.72	−0.47
100–200	0.58	23.34	7.14	4.72	0.66	1.31	1.88
Silt							
0–5	3.47	17.07	9.28	3.11	0.34	0.34	−0.25
5–15	3.47	21.11	9.72	3.90	0.40	0.77	0.35
15–30	2.51	20.04	9.12	3.51	0.38	0.89	1.23
30–60	2.51	17.36	8.61	3.37	0.39	0.55	−0.06
60–100	1.81	17.36	7.98	3.38	0.44	0.77	0.56
100–200	1.58	19.49	7.46	3.83	0.51	1.20	1.67
Sand							
0–5	58.27	90.84	75.45	7.92	0.10	−0.19	−0.85
5–15	46.23	90.97	75.09	9.58	0.13	−0.64	0.08
15–30	52.02	92.99	78.75	9.30	0.12	−0.85	0.36
30–60	64.61	92.42	81.86	7.61	0.09	−0.67	−0.62
60–100	65.10	95.93	84.51	6.91	0.08	−0.89	0.18
100–200	57.16	97.25	85.40	7.90	0.09	−1.57	1.13

3.2. Accuracy Assessment

According to the 10-fold cross-validation results, the R^2 of the predicted values varied from 0.21 to 0.32 (Table 4). Generally speaking, the R^2 of clay, silk, and sand were basically consistent in each layer.

Table 4. Accuracy assessment of the soil particle size distribution predictions.

Depth (cm)	R^2	RMSE (%)	ME (%)
Clay			
0–5	0.21	4.49	0.98
5–15	0.25	4.84	0.89
15–30	0.27	4.68	1.12
30–60	0.32	4.19	1.08
60–100	0.24	4.01	0.90
100–200	0.26	4.43	1.27
Silt			
0–5	0.30	2.91	0.58
5–15	0.21	3.67	0.65
15–30	0.32	2.01	0.67
30–60	0.28	2.75	0.60
60–100	0.25	3.19	0.64
100–200	0.23	3.61	0.79
Sand			
0–5	0.28	6.56	0.25
5–15	0.21	7.82	0.71
15–30	0.24	7.15	0.66
30–60	0.31	5.83	0.23
60–100	0.26	6.58	0.44
100–200	0.23	7.62	0.52

3.3. Spatial Distribution of Soil Particle Size

In terms of spatial distribution, the content of clay and silt showed a decreasing trend with increasing depth, while the content of sand showed an increasing trend, which is consistent with the statistical results (Table 3). For the spatial distribution, the high values of clay and silt were mainly distributed in the southeast of the study area, and the low values were mainly distributed in the northwest of the study area, while sand showed the opposite spatial distribution; that is, the high values of sand were mainly distributed in the northwest, and the low values were mainly distributed in the southeast (Figures 3–5).

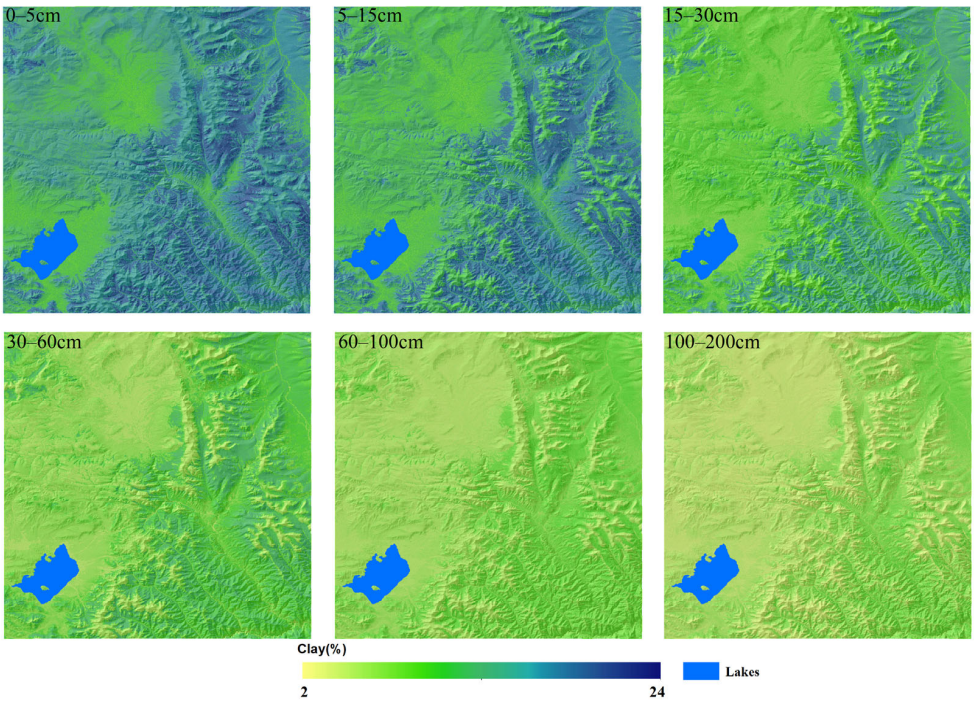

Figure 3. Clay content distribution across six distinct soil depth levels.

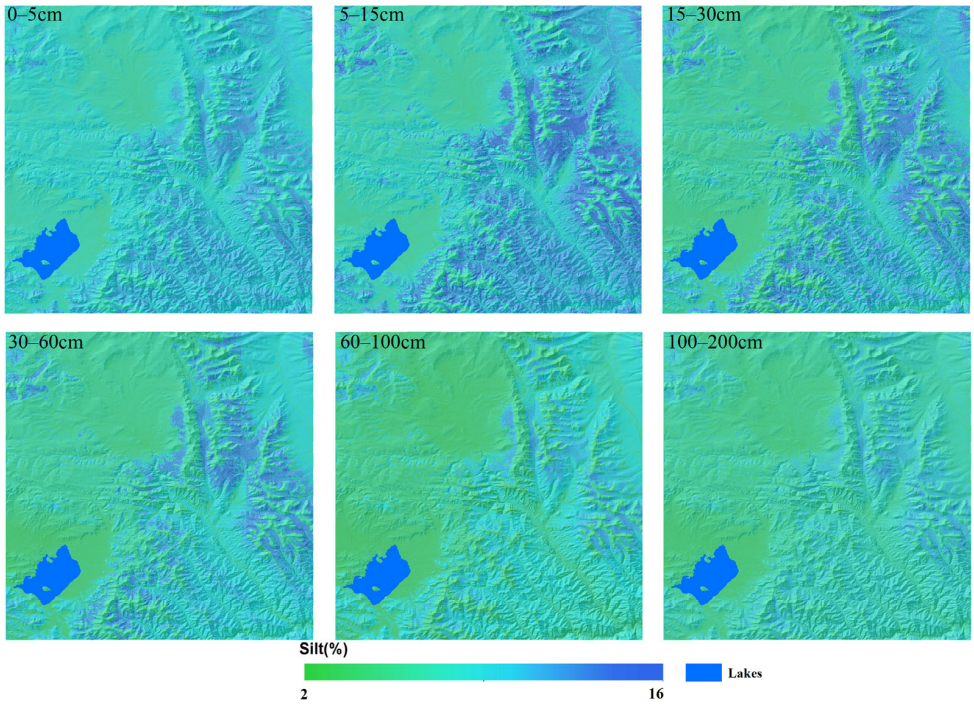

Figure 4. Silt content distribution across six distinct soil depth levels.

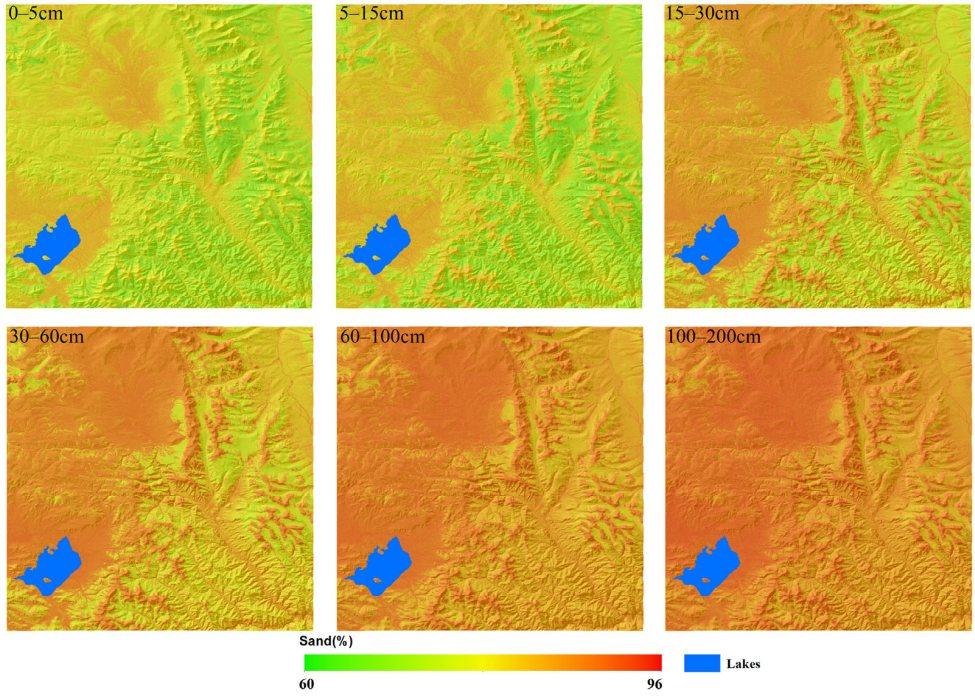

Figure 5. Sand content distribution across six distinct soil depth levels.

3.4. Importance of the Variables

Overall, NDVI and EVI were the main environmental factors controlling the spatial distribution of soil texture in Wenquan area (Figures 6–8). For clay, silt, and sand, as the profile depth increased, their main controlling environmental factors did not change significantly. For the surface clay content within the 0–30 cm depth range, in addition to NDVI and EVI, slope, MAP, and MAT were identified as significant environmental variables influencing the spatial distribution (Figure 6). For silt in 0–5 cm, in addition to NDVI and EVI, MAT and MAP also played an important role. In the range of 5–60 cm, topographic factors played an important role (Figure 7). For sand, in the range of 0–15 cm,

in addition to NDVI and EVI, slope and MAP were the main environmental factors, while in deep layers (15–200 cm), topographic factors were also important influencing factors (Figure 8).

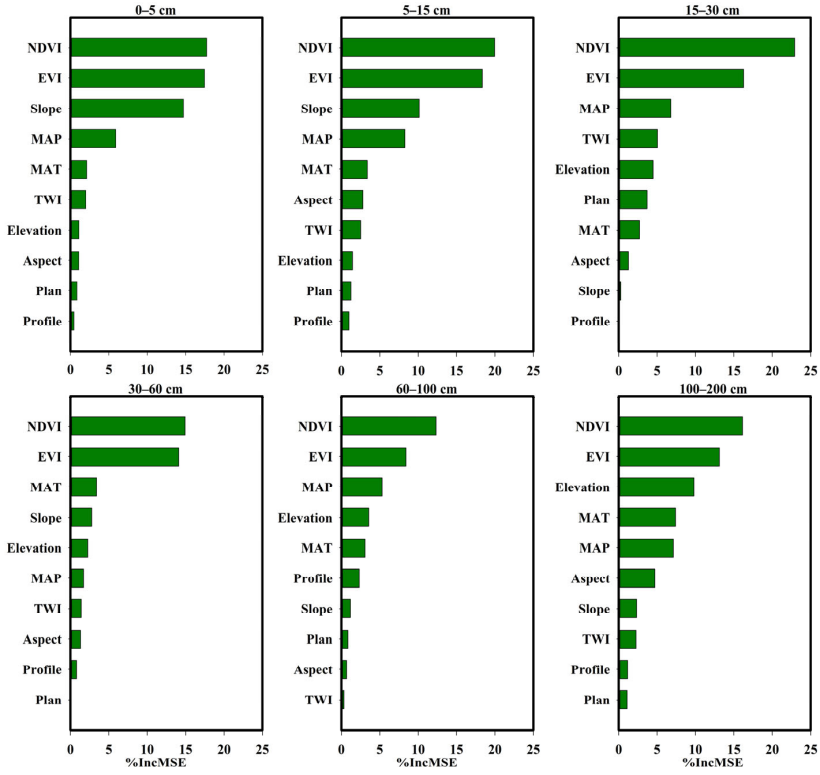

Figure 6. The ranking of the significance of environmental factors affecting clay across various layers.

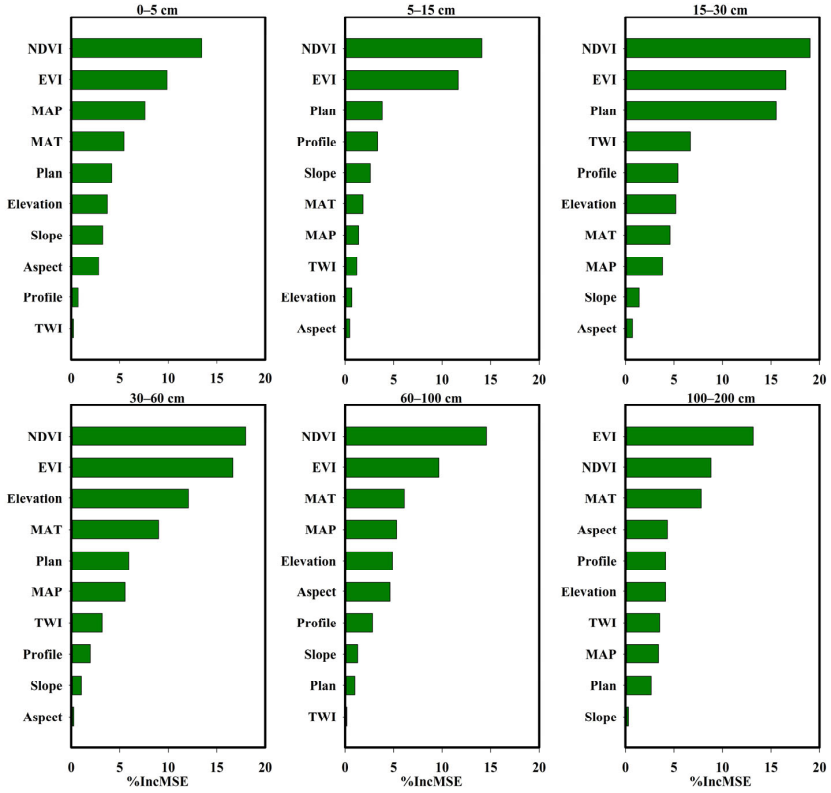

Figure 7. The ranking of the significance of environmental factors affecting silt across various layers.

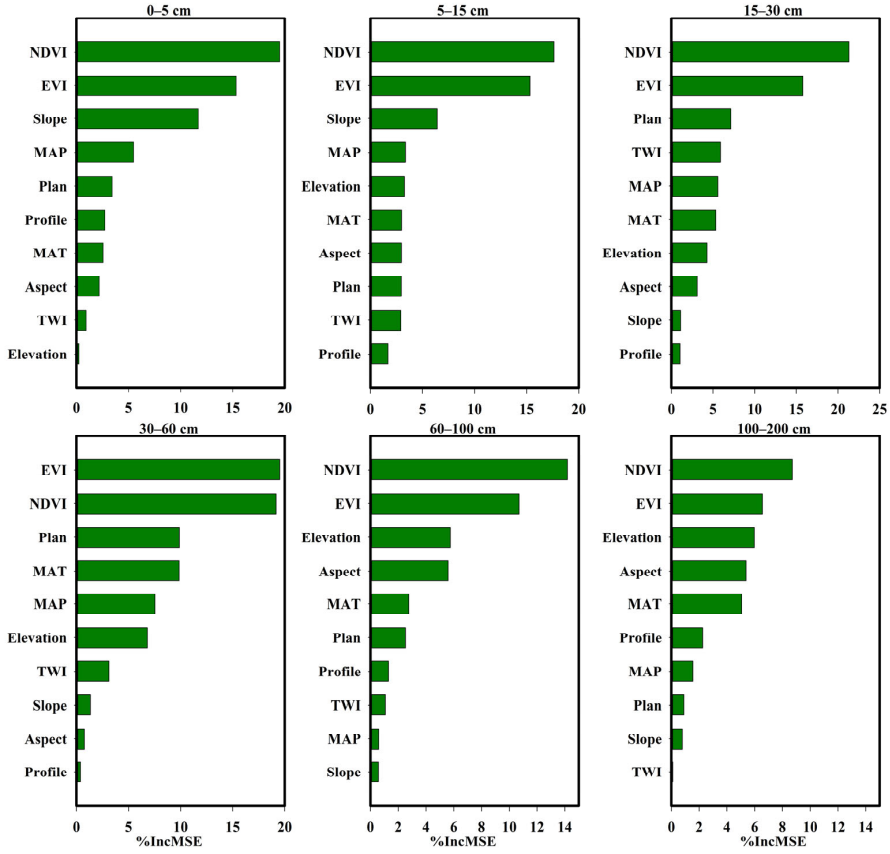

Figure 8. The ranking of the significance of environmental factors affecting sand across various layers.

4. Discussion

In the Wenquan area, the soil particle composition primarily consists of large sand particles, which make up over 75% of the total content, while the amounts of silt and clay are comparatively low. The soil texture in our study area was dominated by sand, which can be explained by the low temperature, low annual precipitation, and sparse vegetation cover in this area because such conditions usually lead to a low soil development rate [48]. The predominant soil type in the study area is Cambosols, characterized by coarse soil particle fractions [35]. Therefore, the soil particle composition is mainly composed of large sand particles.

In the profile distribution of soil texture across different standard layers, the amounts of silt and clay progressively decrease with greater depth, whereas sand exhibits an inverse spatial distribution. This pattern is in agreement with the knowledge that coarse particles are usually higher in deeper layers [49]. This is mainly because the soil-forming parent material in the Wenquan area is relatively simple, mainly composed of slope deposits and alluvial deposits, and the terrain of the study area is complex. Under the action of surface water flow, fine particles of silt and clay are more likely to be suspended and migrated away, and large particles of sand are easier to deposit. Therefore, the sand content will gradually increase in the soil profile. Our study reveals significant lithological differences among soil types and depths in the Wenquan area. Each soil type undergoes distinct weathering and leaching processes during soil formation, leading to unique vertical variations in particle size. For instance, in Typic Haplorthox soils, prolonged leaching results in the accumulation of fine particles, such as clay and silt, in the surface layers, while coarser particles dominate deeper layers. This distribution pattern is primarily driven by the combined effects of gravitational and hydrodynamic forces, creating pronounced particle size contrasts between surface and subsurface horizons. Moreover, the vertical distribution of soil texture is strongly associated with the weathering extent of the parent material, the intensity of leaching processes, and the vertical transport of sediment particles. In colluvial

soils, where the parent material has a relatively simple composition and is shaped by topographic influences, gravitational settling plays a more prominent role, facilitating the accumulation of coarse particles in the lower layers. These processes collectively contribute to the distinctive vertical soil texture patterns observed across different soil types in the study area. From the perspective of spatial distribution, clay, and silt exhibit greater spatial consistency, generally reflecting a trend of higher values in the southeast and lower in the northwest, whereas sand displays a contrasting spatial distribution. This is primarily due to the fact that the northwestern region of the study area has higher elevation, lower temperatures, reduced precipitation, and less developed soil.

The validation results showed that the R^2 values of the predictions of soil texture fraction ranged from 0.21 to 0.32 in this study. The R^2 value is at the medium interpretation level, which is mainly due to the difficulty in obtaining field-measured data and the uneven distribution of sample points due to factors such as terrain, climate, and transportation accessibility. In machine learning models, model accuracy depends on the number and quality of samples. In order to obtain soil particle size distribution at a regional scale, many studies have been performed to improve the accuracy of interpolation such as data transformation prior to kriging [50,51]. Using the random forest model, the combined environmental predictors explained 16~53%, 21~48%, and 21~26% of the total variances in clay, sand, and silt contents, respectively, in Nigeria [52]. Using the equal-area quadratic splines, the predicted accuracy of silt decreased with depth, with the R^2 values of 0.54 for 0–5 cm and 0.29 for 100–200 cm [53]. In our study, the R^2 values were similar to previous reports [54–56], while the R^2 values had no clear difference for the different depths, suggesting that the random forest model is applicable to obtain soil particle size distribution and this method probably can overcome the shortcomings of soil particle size prediction in deep layers using other interpolation methods.

Overall, NDVI and EVI appear to be strongly associated with the spatial distribution of soil texture in the study area; they likely reflect the feedback effect of soil properties on vegetation growth [57,58]. Vegetation affects soil formation through root activity, organic matter input, and biological interactions [59,60]. However, it is also important to consider that changes in NDVI and EVI may be indicative of underlying soil conditions, as finer textures with better moisture retention capacity can enhance vegetation lushness and, consequently, NDVI and EVI values [61]. In our study area, southeastern basins with flatter terrain and finer soil textures (rich in clay and silt) generally exhibit higher NDVI and EVI values, suggesting more vegetation development. Conversely, the mountainous northwest, with coarser soil textures and greater topographical variability, shows poorer vegetation growth and lower NDVI values [62]. Therefore, the soil texture in the southeastern part of the study area is dominated by fine-grained clay and silt, which is consistent with our results. By understanding these pedological dynamics, we can better interpret NDVI and EVI as indicators of soil texture-related moisture conditions across the study area.

Along with NDVI and EVI, which are the key factors influencing the spatial distribution of soil texture in the study area, topography, MAT, and MAP also play a role in this distribution. Topography plays an important role in the formation and distribution of soil texture by affecting the spatial distribution of vegetation. In mountainous areas, vegetation types at different altitudes may show obvious changes, forming vertical vegetation belts [63,64]. The study area lies within a permafrost region, where permafrost in Wenquan covers approximately 75% of the entire area, characterized by varied terrain and a significant altitude gradient. With the increase in altitude, the temperature and climate conditions will change, which will affect the vegetation type and the composition of vegetation communities. Average annual temperature has a direct impact on the formation of soil texture and soil processes. In general, higher mean annual temperatures usually accelerate the chemical weathering process, causing mineral particles to gradually break up and weather, thereby affecting the particle size and texture composition in the soil. The mean annual temperature has an important influence on the growth rate of plants [65]. The study area experiences a low annual average temperature, leading to minimal soil

development. The average annual precipitation also has an important influence on the formation and evolution of soil texture [66]. Adequate precipitation supports vegetation growth and organic matter accumulation, influencing soil formation and texture composition. Increased precipitation can promote the aggregation of clay and silt particles, whereas lower precipitation may result in particle weathering and migration.

5. Conclusions

Our study examined the spatial distribution of soil particle distribution in a permafrost region on the Qinghai–Tibet Plateau. The main controlling factors of soil texture distribution were also examined using the random forest model. Our results showed that sand content was the highest, accounting for more than 75% of the total content. The average values of clay and silt decrease with increasing profile depth, and sand shows the opposite pattern. In terms of spatial distribution, clay and silt have a high degree of synergy, with high levels in the southeast and low levels in the northwest, while sand is just the opposite. The forest model showed that the vegetation cover was the controlling factor for the soil particle distribution. In conclusion, our study showed that random forest is a useful tool to predict spatial distribution of soil particle sizes for areas with complex terrains.

Author Contributions: Conceptualization, W.L. and Y.L.; methodology, D.Z. and Y.Q.; software, Y.L.; validation, T.W. and L.Z.; formal analysis, Y.L.; investigation, G.H. and X.W. (Xiaoxian Wang); resources, X.W. (Xiaodong Wu); data curation, X.F.; writing—original draft preparation, Y.L.; writing—review and editing, W.L.; visualization, D.Z.; supervision, T.W.; project administration, X.W. (Xiaodong Wu); funding acquisition, X.W. (Xiaodong Wu) and W.L. All authors have read and agreed to the published version of the manuscript.

Funding: This work was financially supported by the Gansu Provincial Science and Technology Program (22ZD6FA005), National Natural Science Foundation of China (U23A2062, 32361133551, 41601066).

Data Availability Statement: All the derived data based on these original data sources are available from the corresponding author upon reasonable request.

Acknowledgments: We thank our colleagues for their insightful comments on an earlier version of this manuscript.

Conflicts of Interest: The authors declare no conflicts of interest.

References

1. Richer-De-Forges, A.C.; Arrouays, D.; Poggio, L.; Songchao, C.; Lacoste, M.; Minasny, B.; Libohova, Z.; Roudier, P.; Mulder, V.L.; Nédélec, H.J.P. Hand-feel soil texture observations to evaluate the accuracy of digital soil maps for local prediction of soil particle size distribution: A case study in Central France. *Pedosphere* **2023**, *33*, 731–743. [CrossRef]
2. Siqueira, R.G.; Moquedace, C.M.; Francelino, M.R.; Schaefer, C.E.; Fernandes-Filho, E.I.J.G. Machine learning applied for Antarctic soil mapping: Spatial prediction of soil texture for Maritime Antarctica and Northern Antarctic Peninsula. *Geoderma* **2023**, *432*, 116405. [CrossRef]
3. Moreno-Maroto, J.M.; Alonso-Azcárate, J.J. Evaluation of the USDA soil texture triangle through Atterberg limits and an alternative classification system. *Appl. Clay Sci.* **2022**, *229*, 106689. [CrossRef]
4. Kaya, F.; Başayiğit, L. Spatial prediction and digital mapping of soil texture classes in a floodplain using multinomial logistic regression. In *Intelligent and Fuzzy Techniques for Emerging Conditions and Digital Transformation, Proceedings of the INFUS 2021 Conference, Istanbul, Turkey, 24–26 August 2021*; Springer: Berlin/Heidelberg, Germany, 2022; Volume 2.
5. Wang, Z.; Li, W.; Li, W.; Yang, W.; Jing, S.J.C. Effects of microplastics on the water characteristic curve of soils with different textures. *Chemosphere* **2023**, *317*, 137762. [CrossRef]
6. Wessolek, G.; Bohne, K.; Trinks, S.T. Validation of soil thermal conductivity models. *Int. J. Thermophys.* **2023**, *44*, 20. [CrossRef]
7. Johannes, A.; Sauzet, O.; Matter, A.; Boivin, P. Soil organic carbon content and soil structure quality of clayey cropland soils: A large-scale study in the Swiss Jura region. *Soil Use Manag.* **2023**, *39*, 707–716. [CrossRef]
8. Naz, B.S.; Sharples, W.; Ma, Y.; Goergen, K.; Kollet, S. Continental-scale evaluation of a fully distributed coupled land surface and groundwater model, ParFlow-CLM (v3. 6.0), over Europe. *Geosci. Model Dev.* **2023**, *16*, 1617–1639. [CrossRef]
9. Ngu, N.H.; Thanh, N.N.; Duc, T.T.; Non, D.Q.; An, N.T.T.; Chotpantarat, S. Active learning-based random forest algorithm used for soil texture classification mapping in Central Vietnam. *Catena* **2024**, *234*, 107629. [CrossRef]

10. Talebmorad, H.; Ostad-Ali-Askari, K. Hydro geo-sphere integrated hydrologic model in modeling of wide basins. *Sustain. Water Resour. Manag.* **2022**, *8*, 118. [CrossRef]
11. Smith, S.L.; O'Neill, H.B.; Isaksen, K.; Noetzli, J.; Romanovsky, V. The changing thermal state of permafrost. *Nat. Rev. Earth Environ.* **2022**, *3*, 10–23. [CrossRef]
12. Obu, J.; Westermann, S.; Bartsch, A.; Berdnikov, N.; Christiansen, H.H.; Dashtseren, A.; Delaloye, R.; Elberling, B.; Etzelmüller, B.; Kholodov, A. Northern Hemisphere permafrost map based on TTOP modelling for 2000–2016 at 1 km^2 scale. *Earth-Sci. Rev.* **2019**, *193*, 299–316. [CrossRef]
13. Yin, G.-A.; Luo, J.; Niu, F.-J.; Liu, M.-H.; Gao, Z.-Y.; Dong, T.-C.; Ni, W. Environmental factors controlling soil warming and wetting during 2000–2020 in permafrost and non-permafrost regions across the Qinghai–Tibet Plateau. *Adv. Clim. Chang. Res.* **2024**, *15*, 285–296. [CrossRef]
14. Biskaborn, B.K.; Smith, S.L.; Noetzli, J.; Matthes, H.; Vieira, G.; Streletskiy, D.A.; Schoeneich, P.; Romanovsky, V.E.; Lewkowicz, A.G.; Abramov, A. Permafrost is warming at a global scale. *Nat. Commun.* **2019**, *10*, 264. [CrossRef] [PubMed]
15. O'Neill, H.; Smith, S.; Burn, C.; Duchesne, C.; Zhang, Y. Widespread permafrost degradation and thaw subsidence in northwest Canada. *J. Geophys. Res. Earth Surf.* **2023**, *128*, e2023JF007262. [CrossRef]
16. Svennevig, K.; Keiding, M.; Korsgaard, N.J.; Lucas, A.; Owen, M.; Poulsen, M.D.; Priebe, J.; Sørensen, E.V.; Morino, C. Uncovering a 70-year-old permafrost degradation induced disaster in the Arctic, the 1952 Niiortuut landslide-tsunami in central West Greenland. *Sci. Total Environ.* **2023**, *859*, 160110. [CrossRef]
17. Murton, J.B. Permafrost and Climate Change. In *Climate Change*; Elsevier: Amsterdam, The Netherlands, 2021; pp. 281–326.
18. Schuur, E.A.; Abbott, B.W.; Commane, R.; Ernakovich, J.; Euskirchen, E.; Hugelius, G.; Grosse, G.; Jones, M.; Koven, C.; Leshyk, V. Permafrost and climate change: Carbon cycle feedbacks from the warming Arctic. *Annu. Rev. Environ. Resour.* **2022**, *47*, 343–371. [CrossRef]
19. Zhao, L.; Hu, G.; Liu, G.; Zou, D.; Wang, Y.; Xiao, Y.; Du, E.; Wang, C.; Xing, Z.; Sun, Z.; et al. Investigation, Monitoring, and Simulation of Permafrost on the Qinghai-Tibet Plateau: A Review. *Permafr. Periglac. Process.* **2024**, *35*, 412–422. [CrossRef]
20. Li, H.; Bulcke, J.V.D.; Mendoza, O.; Deroo, H.; Haesaert, G.; Dewitte, K.; De Neve, S.; Sleutel, S. Soil texture controls added organic matter mineralization by regulating soil moisture—Evidence from a field experiment in a maritime climate. *Geoderma* **2022**, *410*, 115690. [CrossRef]
21. Zhou, Y.; Wu, W.; Wang, H.; Zhang, X.; Yang, C.; Liu, H. Identification of soil texture classes under vegetation cover based on Sentinel-2 data with SVM and SHAP techniques. *IEEE J. Sel. Top. Appl. Earth Obs. Remote Sens.* **2022**, *15*, 3758–3770. [CrossRef]
22. Wang, Q.; Wen, Y.; Zhao, B.; Hong, H.; Liao, R.; Li, J.; Liu, J.; Lu, H.; Yan, C. Coastal soil texture controls soil organic carbon distribution and storage of mangroves in China. *Catena* **2021**, *207*, 105709. [CrossRef]
23. Mei, Q.-H.; Chen, J.; Liu, Y.-Q.; Zhang, S.-H.; Zhao, J.-Y.; Dong, T.-C.; Wang, J.-C.; Zhao, Y. Degradation of warm permafrost and talik formation on the Qinghai–Tibet Plateau in 2006–2021. *Adv. Clim. Chang. Res.* **2024**, *15*, 275–284. [CrossRef]
24. Zakharov, M.; Gadal, S.; Kamičaitytė, J.; Cherosov, M.; Troeva, E. Distribution and Structure Analysis of Mountain Permafrost Landscape in Orulgan Ridge (Northeast Siberia) Using Google Earth Engine. *Land* **2022**, *11*, 1187. [CrossRef]
25. Zou, D.; Zhao, L.; Sheng, Y.; Chen, J.; Hu, G.; Wu, T.; Wu, J.; Xie, C.; Wu, X.; Pang, Q.; et al. A new map of permafrost distribution on the Tibetan Plateau. *Cryosphere* **2017**, *11*, 2527–2542. [CrossRef]
26. Shangguan, W.; Dai, Y.; Liu, B.; Ye, A.; Yuan, H. A soil particle-size distribution dataset for regional land and climate modelling in China. *Geoderma* **2012**, *171*, 85–91. [CrossRef]
27. Mitran, T.; Solanky, V.; Suresh, G.J.; Sujatha, G.; Sreenivas, K.; Ravisankar, T. Predictive mapping of surface soil texture in a semiarid region of India through geostatistical modeling. *Model. Earth Syst. Environ.* **2019**, *5*, 645–657. [CrossRef]
28. Liao, K.; Xu, S.; Wu, J.; Zhu, Q. Spatial estimation of surface soil texture using remote sensing data. *Soil Sci. Plant Nutr.* **2013**, *59*, 488–500. [CrossRef]
29. Chen, S.; Arrouays, D.; Mulder, V.L.; Poggio, L.; Minasny, B.; Roudier, P.; Libohova, Z.; Lagacherie, P.; Shi, Z.; Hannam, J. Digital mapping of GlobalSoilMap soil properties at a broad scale: A review. *Geoderma* **2022**, *409*, 115567. [CrossRef]
30. Schulz, G.; Rodriguez, D.M.; Angelini, M.; Moretti, L.M.; Olmedo, G.F.; Vuegen, L.M.T.; Colazo, J.C.; Guevara, M. Digital soil texture maps of Argentina and their relationship to soil-forming factors and processes. In *Geopedology: An Integration of Geomorphology and Pedology for Soil and Landscape Studies*; Springer: Berlin/Heidelberg, Germany, 2023; pp. 263–281.
31. McBratney, A.B.; Santos, M.M.; Minasny, B.J.G. On digital soil mapping. *Geoderma* **2003**, *117*, 3–52. [CrossRef]
32. Liu, F.; Zhang, G.-L.; Song, X.; Li, D.; Zhao, Y.; Yang, J.; Wu, H.; Yang, F. High-resolution and three-dimensional mapping of soil texture of China. *Geoderma* **2020**, *361*, 114061. [CrossRef]
33. Arrouays, D.; Grundy, M.G.; Hartemink, A.E.; Hempel, J.W.; Heuvelink, G.B.; Hong, S.Y.; Lagacherie, P.; Lelyk, G.; McBratney, A.B.; McKenzie, N.J. GlobalSoilMap: Toward a fine-resolution global grid of soil properties. *Adv. Agron.* **2014**, *125*, 93–134.
34. Omondiagbe, O.P.; Lilburne, L.; Licorish, S.A.; MacDonell, S. Soil texture prediction with automated deep convolutional neural networks and population-based learning. *Geoderma* **2023**, *436*, 116521. [CrossRef]
35. Li, W.; Zhao, L.; Wu, X.; Wang, S.; Sheng, Y.; Ping, C.; Zhao, Y.; Fang, H.; Shi, W. Soil distribution modeling using inductive learning in the eastern part of permafrost regions in Qinghai–Xizang (Tibetan) Plateau. *Catena* **2015**, *126*, 98–104. [CrossRef]
36. Svensson, D.N.; Messing, I.; Barron, J.J.S. An investigation in laser diffraction soil particle size distribution analysis to obtain compatible results with sieve and pipette method. *Soil Tillage Res.* **2022**, *223*, 105450. [CrossRef]

37. Cui, P.; Chen, Z.; Fan, F.; Yin, C.; Song, A.; Li, T.; Zhang, H.; Liang, Y. Soil texture is an easily overlooked factor affecting the temperature sensitivity of N2O emissions. *Sci. Total Environ.* **2023**, *862*, 160648. [CrossRef]
38. Jenny, H. *The Soil Resource: Origin and Behavior*; Springer Science & Business Media: Berlin/Heidelberg, Germany, 2012.
39. Breiman, L.J. Random forests. *Mach. Learn.* **2001**, *45*, 5–32. [CrossRef]
40. Asif, M.; Kazmi, J.H.; Tariq, A.; Zhao, N.; Guluzade, R.; Soufan, W.; Almutairi, K.F.; Sabagh, A.E.; Aslam, M. Modelling of land use and land cover changes and prediction using CA-Markov and Random Forest. *Geocarto Int.* **2023**, *38*, 2210532. [CrossRef]
41. Sihag, P.; Angelaki, A.; Chaplot, B. Estimation of the recharging rate of groundwater using random forest technique. *Appl. Water Sci.* **2020**, *10*, 182. [CrossRef]
42. Loozen, Y.; Rebel, K.T.; de Jong, S.M.; Lu, M.; Ollinger, S.V.; Wassen, M.J.; Karssenberg, D.J. Mapping canopy nitrogen in European forests using remote sensing and environmental variables with the random forests method. *Remote Sens. Environ.* **2020**, *247*, 111933. [CrossRef]
43. Bargués-Tobella, A.; Winowiecki, L.A.; Sheil, D.; Vågen, T. Determinants of Soil Field-Saturated Hydraulic Conductivity Across Sub-Saharan Africa: Texture and Beyond. *Copernic. Meet.* **2024**, *60*, e2023WR035510. [CrossRef]
44. Eymard, A.; Richer-de-Forges, A.C.; Martelet, G.; Tissoux, H.; Bialkowski, A.; Dalmasso, M.; Chrétien, F.; Belletier, D.; Ledemé, G.; Laloua, D.J. Exploring the untapped potential of hand-feel soil texture data for enhancing digital soil mapping: Revealing hidden spatial patterns from field observations. *Geoderma* **2024**, *441*, 116769. [CrossRef]
45. Amsili, J.P.; van Es, H.M.; Schindelbeck, R. Pedotransfer Functions for Field Capacity, Permanent Wilting Point, and Available Water Capacity Based on Random Forest Models for Routine Soil Health Analysis. *Commun. Soil Sci. Plant Anal.* **2024**, *55*, 1967–1984. [CrossRef]
46. Kaveh, N.; Ebrahimi, A.; Asadi, E. Comparative analysis of random forest, exploratory regression, and structural equation modeling for screening key environmental variables in evaluating rangeland above-ground biomass. *Ecol. Inform.* **2023**, *77*, 102251. [CrossRef]
47. Bognounou, F.; Paré, D.; Laganière, J. Changes in seedlings' composition and abundance following soil scarification and amendments in a northern hardwood forest. *For. Ecol. Manag.* **2023**, *541*, 121071. [CrossRef]
48. Chou, Y.; Sheng, Y.; Wei, Z. Temperature and deformation differences between southern and northern slopes of highway embankment on permafrost. *J. Rock Mech. Eng.* **2009**, *28*, 1896–1903.
49. Cuo, L.; Zhao, H.; Zhang, Y.; Li, N.; Liang, L.; Liu, Z.; Ding, J.; Zhu, F. Spatiotemporally heterogeneous soil thermohydraulic processes in the frozen soil of the Tibetan Plateau. *Geoderma* **2023**, *438*, 116634. [CrossRef]
50. Saurette, D. Comparing direct and indirect approaches to predicting soil texture class. *Can. J. Soil Sci.* **2022**, *102*, 835–851. [CrossRef]
51. Shi, W.; Zhang, M. Progress on spatial prediction methods for soil particle-size fractions. *J. Geogr. Sci.* **2023**, *33*, 1553–1566. [CrossRef]
52. Akpa, S.I.; Odeh, I.O.; Bishop, T.F.; Hartemink, A.E. Digital mapping of soil particle-size fractions for Nigeria. *Soil Sci. Soc. Am. J.* **2014**, *78*, 1953–1966. [CrossRef]
53. Adhikari, K.; Kheir, R.B.; Greve, M.B.; Bøcher, P.K.; Malone, B.P.; Minasny, B.; McBratney, A.B.; Greve, M. High-resolution 3-D mapping of soil texture in Denmark. *Soil Sci. Soc. Am. J.* **2013**, *77*, 860–876. [CrossRef]
54. Rossel, R.V.; Chen, C.; Grundy, M.; Searle, R.; Clifford, D.; Campbell, P. The Australian three-dimensional soil grid: Australia's contribution to the GlobalSoilMap project. *Soil Res.* **2015**, *53*, 845–864. [CrossRef]
55. Mulder, V.L.; Lacoste, M.; Richer-de-Forges, A.C.; Arrouays, D. GlobalSoilMap France: High-resolution spatial modelling the soils of France up to two meter depth. *Sci. Total Environ.* **2016**, *573*, 1352–1369. [CrossRef] [PubMed]
56. Padarian, J.; Minasny, B.; McBratney, A. Chile and the Chilean soil grid: A contribution to GlobalSoilMap. *Geoderma Reg.* **2017**, *9*, 17–28. [CrossRef]
57. Kumar, P.; Kumar, P.; Verma, V.; Irfan, M.; Sharma, R.; Bhargava, B. How plants conquered land: Evolution of terrestrial adaptation. *J. Evol. Biol.* **2023**, *35*, 5–14.
58. Kammann, S.; Leinweber, P.; Glaser, K.; Schiefelbein, U.; Dolnik, C.; Mikhailyuk, T.; Demchenko, E.; Heilmann, E.; Karsten, U. Successional development of the phototrophic community in biological soil crusts, along with soil formation on Holocene deposits at the Baltic Sea coast. *Front. Ecol. Evol.* **2024**, *11*, 1266209. [CrossRef]
59. Wang, P.; Su, X.; Zhou, Z.; Wang, N.; Zhu, B. Differential effects of soil texture and root traits on the spatial variability of soil infiltrability under natural revegetation in the Loess Plateau of China. *Catena* **2023**, *220*, 106693. [CrossRef]
60. Kartalaei, Z.M.; Kooch, Y.; Tilaki, G. Litter and soil properties under woody and non-woody vegetation types: Implication for ecosystem management in a mountainous semi-arid landscape. *J. Environ. Manag.* **2023**, *348*, 119238. [CrossRef]
61. Felegari, S.; Sharifi, A.; Moravej, K.; Golchin, A.; Tariq, A. Investigation of the relationship between ndvi index, soil moisture, and precipitation data using satellite images. *Sustain. Agric. Syst. Technol.* **2022**, *2022*, 314–325.
62. Zhang, X.; Nan, Z.; Wu, J.; Du, E.; Wang, T.; You, Y.; Regions, A. Mountain permafrost distribution modeling using Multivariate Adaptive Regression Spline (MARS) in the Wenquan area over the Qinghai-Tibet Plateau. *Sci. Cold Arid Reg.* **2012**, *4*, 361–370.
63. Zhao, T.; Bai, H.; Han, H.; Ta, Z.; Li, P.; Wang, P. A Quantitatively Divided Approach for the Vertical Belt of Vegetation Based on NDVI and DEM—An Analysis of Taibai Mountain. *Forests* **2023**, *14*, 1981. [CrossRef]
64. Volkov, I.; Volkova, I. Are There Mountain Xerphytes in the Mountains of South Siberia? *Arid Ecosyst.* **2023**, *13*, 395–402. [CrossRef]

65. Wei, G.; Weisai, L.; Zhou, Z.; Wu, X.; Gao, S.; Fu, Z.; Wu, Q.; Jiang, G. Impact of a retrogressive thaw slump on surrounding vegetation communities in the Fenghuoshan mountains, Qinghai-Tibet Plateau. *Res. Cold Arid Reg.* **2023**, *15*, 11–17. [CrossRef]
66. Sun, X.; Li, S.; Zhai, X.; Wei, X.; Yan, C. Ecosystem changes revealed by land cover in the three-river headwaters region of Qinghai, China (1990–2015). *Res. Cold Arid Reg.* **2023**, *15*, 85–91. [CrossRef]

Disclaimer/Publisher's Note: The statements, opinions and data contained in all publications are solely those of the individual author(s) and contributor(s) and not of MDPI and/or the editor(s). MDPI and/or the editor(s) disclaim responsibility for any injury to people or property resulting from any ideas, methods, instructions or products referred to in the content.